Surface & Coatings Technology 232 (2013) 131–141

Contents lists available at ScienceDirect

Surface & Coatings Technology

journal homepage: www.elsevier.com/locate/surfcoat

Anticorrosion and nanomechanical performance of hybrid organo-silicate coatings integrating corrosion inhibitors

E. Roussi [a], A. Tsetsekou [a,*], A. Skarmoutsou [b], C.A. Charitidis [b], A. Karantonis [b]

[a] School of Mining Engineering & Metallurgy, National Technical University of Athens, 9 Iroon Polytechniou, Zografou Campus, 15780 Athens, Greece
[b] School of Chemical Engineering, National Technical University of Athens, 9 Iroon Polytechniou, Zografou Campus, 15780 Athens, Greece

ARTICLE INFO

Article history:
Received 11 December 2012
Accepted in revised form 29 April 2013
Available online 8 May 2013

Keywords:
Coatings
Corrosion
AA2024-T3 alloy
Sol–gel
Hyperbranched poly(ethylene imine)
Nanomechanical evaluation

ABSTRACT

Corrosion protective sol–gel silica coatings were developed on AA2024-T3 alloy by in situ cross-linking with hyperbranched poly(ethylene imine). Coatings with or without corrosion inhibitors (2-mercaptobenzothiazole or 2-mercaptobenzimidazole) and of two different thicknesses (1–1.5 and 3–3.5 μm, respectively) were obtained. Potentiodynamic scans and electrochemical impedance spectroscopy (after immersion in Harrison's solution for up to 4 weeks) were employed to evaluate the anticorrosion performance of coatings, whereas their thickness, morphology and integrity were assessed by scanning electron microscopy and atomic force microscopy. Further the depth sensing nanoindentation technique was employed to measure the hardness and reduced modulus of coatings and the obtained data were analyzed to indicate their wear resistance, plastic deformation and mechanical integrity. In all cases, coatings of high quality with good barrier properties (impedance modulus reaching up to 10^6 Ω cm^2 at the very low frequency regime) and self-healing abilities (in case of the inclusion of an inhibitor) were obtained. The coating thickness was found to affect the anticorrosion performance, however, even thinner coatings demonstrate satisfactory protection and self-healing effect. Nanoindentation analysis revealed the flexible nature and viscous behavior of the coatings (with the theoretical transition of the elastic to plastic behavior appearing at 1000 μN applied load) demonstrating also an optimal integration of the organic inhibitors into the film. It also revealed an effect of thickness with thinner coatings exhibiting slightly superior behavior in terms of elasticity and wear resistance.

1. Introduction

In contrast to pure aluminum, alloys containing copper, magnesium and silicon as the principal substitution elements are susceptible to atmospheric corrosion. Some aluminum alloys such as AA2024-T3 present severe pitting and develop a voluminous white corrosion product under some exposure conditions in corrosive atmosphere. Chromate conversion coatings offer very good corrosion protection for aluminum alloys. However, due to the carcinogenic toxicity of hexavalent chromium (Cr^{6+}), alternatively, environmentally friendly techniques are preferable. A promising technology for anticorrosion coatings is sol–gel, as it provides thin films with good adhesion in both metallic substrates and organic top coats. Sol–gel hybrid organic–inorganic thin films have been successful in several areas such as adhesion improvement [1,2] responsive coatings, and anticorrosion protection [3].

The beneficial adhesion properties of sol–gel based coatings to metals are due to the fact that strong covalent Si–O–Me bonds are formed [4,5]. In particular water-based organofunctional silanes have displayed interfacial adhesion between the inorganic colloidal surface as well as structural strength attributed to a crosslinking network formation. In general though, sol–gel films do not demonstrate extensive anticorrosion properties and may fail to protect the metal surface from the formation of defects such as micropores and cracks during the drying process [6,7]. To improve anti-corrosion properties, inhibitor-doped sol–gel formulations [8–10] are being recently investigated. Those are expected to reduce the rate of the corrosion process and may also demonstrate "self-healing" anticorrosion properties [11]. However, the importance of inhibitor incorporation is not clearly established. Additionally, it has been noted that inhibitors can also have a negative impact on the stability and consequently, sol–gel films exhibit barrier properties [12], while the release of inhibitors from coatings is often fast and not controllable.

Recent research focuses on encapsulating and complexating the inhibitor in suitable nanoreservoirs in order to avoid the direct interaction with the sol–gel matrix and to also achieve its slow release. In order to accomplish this goal, the inclusion of an inhibitor in nanoparticles [13,14], its encapsulation using a layer by layer approach [15] or its complexation with other molecules such as β-cyclodextrin [16,17] and hyperbranched poly(ethylene imine) (PEI) [18] have been reported. PEI is a highly branched cationic polymer bearing in its branches secondary and primary amino end groups [19]. Due to its chemical structure it can react with epoxides acting as

* Corresponding author. Tel.: +30 210 7722213; fax: +30 210 7722119.
E-mail address: athtse@metal.ntua.gr (A. Tsetsekou).

0257-8972/$ – see front matter © 2013 Elsevier B.V. All rights reserved.
http://dx.doi.org/10.1016/j.surfcoat.2013.04.063

a cross-linking agent for hybrid film formation while, due to its polymeric nature, has also good film forming ability. Moreover, it possesses anti-corrosive properties [20] and finally, as a hyperbranched polymer, it can encapsulate in its interior non-water-soluble organic molecules [21,22]. As a result, hybrid coatings cured with amine present high hardness, essential adherence onto aluminum alloy substrates, exhibit excellent bare and filiform corrosion resistance, and good compatibility with organic polymer paint systems [23].

Another issue concerning the sol–gel anticorrosion coatings is their rather poor mechanical behavior, which depends on structure and composition, inherent mechanical properties of the substrate, adhesion strength, residual stresses and coating thickness [24]. Consequently, it is crucial to investigate the suitability of the synthesized sol–gel anticorrosion coatings in conjunction with their mechanical performance. It is though important to study the mechanical behavior of coatings and the coating–substrate system, in order to measure the hardness and elastic modulus values of the coating and the coating's adhesion onto the substrate. This study can be achieved with the use of the depth sensing nanoindentation technique and the obtained data can be analyzed to indicate the wear resistance and the plastic deformation of the synthesized coatings.

In our previous work, corrosion protective sol–gel coatings were developed on AA2024-T3 alloy through an aqueous sol–gel process which includes in situ formation of a dense silica network from hydrolyzed 3-glycidoxy-propyltri-methoxysilane and tetraethoxysilane followed by in situ cross-linking by hyperbranched PEI [18]. Two organic corrosion inhibitors (2-mercaptobenzothiazole — MBT and 2-mercaptobenzimidazole — MBI) were combined with PEI to induce self-healing properties. The as-developed coatings demonstrated very good anticorrosion performance attributed to the optimal integration of the organic inhibitors in the film inducing self-healing of corrosion defects. In fact, PEI can act as a crosslinking agent for hybrid film formation, and as a solubilizer of organic corrosion inhibitors, being also a corrosion inhibitor by itself contributing thus in a variety of ways to the overall properties of the hybrid film.

In the present study, the same methodology was employed to deposit hybrid organo-silicate coatings onto AA2024-T3 alloy aiming at assessing their anticorrosion protection ability and evaluating their nanomechanical properties, wear resistance and adhesion to the substrate, correlating, in this way, their overall performance with the process parameters. In this respect, coatings integrating or not an organic inhibitor (MBT or MBI) and differing in their thickness, (affected by the dipping time of the alloy into the synthesized cross-linked sol) were developed and the observed differences are discussed.

2. Experimental procedure

2.1. Synthesis of coatings

AA2024-T3 alloy coupons with dimensions of 60 × 20 × 2.45 mm were employed for the application of coatings. The AA2024-T3 alloy is made up of Al, 3.8–4.9 Cu, 1.2–1.5 Mg, 0.3–0.9 Mn, 0.5 Si, 0.5 Fe, 0.1 Cr, Zn and Ti. The AA2024-T3 substrates were cleaned in an alkaline aqueous solution containing 50 g/l of TURCO TM 4215 (TURCO S.A. Spain) for 15 min at 60 C followed by immersion into a 20% v/v HNO_3 (Merck) solution for 15 min and then washed by deionized water. This treatment is industrially applied for AA2024 and leads to partial dissolution of the copper phases which is the cause of the low resistance of the alloy [25].

The sol–gel process involved the preparation of an aqueous solution by the drop-wise addition, under continuous stirring, of 3-glycidoxy-propyltri-methoxysilane (GPTMS) (97% pure, Merck) and tetraethoxysilane (TEOS) (99% pure, Alfa Aesar) in 3:1 molar ratio to a 0.05 M solution of acetic acid (Merck) in deionized water. The resulting silane solution (30.4% v/v and 9.4% v/v in GPTMS and TEOS, respectively) was kept at room temperature under continuous stirring for 3 days in order the hydrolysis and condensation reactions to take place. Then, it was further diluted by a factor of 2 with water and 1% v/v surfactant (Darvan-C, Vanderbilt-USA) was added followed by the addition of the cross-linker agent (hyperbranched polymer poly(ethylene imine) – PEI – of molecular weight 25,000 — Aldrich) to a final concentration of 3.5% w/v. Additionally, sols containing organic corrosion inhibitors were also synthesized in order to incorporate them into the hybrid organo-silicate coatings. For this, 0.115% w/v of 2-mercaptobenzothiazole (MBT, Alfa Aesar) or 0.105% w/v of 2-mercaptobenzimidazole (MBI, Alfa Aesar) were dissolved respectively into the as prepared silane solution prior to the addition of PEI.

Finally, the cleaned AA2024-T3 coupons were dipped into the cross-linked silane solutions (immediately after its preparation) either for 100 s or 300 s, resulting in variations in coating thickness. Controlled ascension with a speed of 10 cm/min was followed and the coated coupons were cured at room temperature for 24 h. The different coatings that were developed in this way are summarized in Table 1.

2.2. Characterization of coatings

The corrosion performance of the coated aluminum samples was studied by potentiodynamic scan (PDS) measurements conducted in Harrison's solution (0.35 wt.% $(NH_4)_2SO_4$ and 0.05 wt.% NaCl) with the aid of a Potentiostat/Galvanostat Model 263A (EG&G, Princeton Applied Research, instrumentation accuracy ± 5 nA). The Harrison's solution emulates the atmospheric conditions of an aircraft [26]. Electrochemical measurements were executed using a one-chamber, three-electrode cell. The reference electrode was a 3 M KCl Ag/AgCl electrode connected through a Luggin capillary, whereas the cathode was a platinum electrode. The experiments were carried out at 20 C employing a scan rate of 0.2 mV/s and each coating system was evaluated in triplicate. Before polarization is applied, coated samples were immersed in the solution for a period of 90 min whereas bare aluminum samples were immersed for 20 min. The Tafel plots were statistically fitted to the Stearn–Geary model for a corroding system by using the Power Corr Software.

The coating quality together with the corrosion behavior was also explored by electrochemical impedance spectroscopy (EIS). Samples dip-coated for 100 s were examined with respect to their corrosion behavior, since thicker coating anticorrosion performance has already been reported in [18]. The EIS measurements were achieved using a Solartron SI 1260, impedance/gain-phase analyzer. The EIS measurements were performed at room temperature using a three-electrode electrochemical cell, consisting of the working electrode (1 cm^2 area), saturated calomel electrode (SCE) as reference and platinum as counter electrode. The measuring frequency ranged from 10^5 Hz down to 10^{-2} Hz. The r.m.s. voltage was 10 mV. The EIS experiments initially were performed after immersion of the coated substrates in Harrison's solution for 72 h, 1, 2, 3 and 4 weeks. Spectra were treated using the Software Zplot/Zview (Scribner Assoc. Inc.)

In addition, scanning electron microscopy (SEM) studies performed in a JEOL JSM 6380-LV instrument were employed to evaluate the thickness, surface morphology and quality of the films developed before and

Table 1
Corrosion inhibitor and dipping period data of the prepared coatings.

Coating code	Corrosion inhibitor	Dip coating time
PEI25000-100	–	100 s
PEI25000-MBI-100	MBI	100 s
PEI25000-MBT-100	MBT	100 s
PEI25000-300	–	300 s
PEI25000-MBI-300	MBI	300 s
PEI25000-MBT-300	MBT	300 s

after the corrosion tests. Energy dispersive X-ray analysis (EDX) was used to characterize and confirm the surface coating in cross section images at an accelerating voltage of 20 kV.

The three-dimensional topography and roughness of the films were evaluated with the aid of an atomic force microscopy (AFM, DME Dualscope DS95).

The indentation analysis was performed using a Hysitron TriboLab® Nanomechanical Test Instrument (Hysitron Inc., Minneapolis, USA) that is capable of performing indentations. The equipment allows the application of loads from 1 to 10,000 μN and the recording of penetration depths as a function of applied loads with a high load resolution (1 nN) and a high displacement resolution (0.04 nm) [27]. A fine calibrated Berkovich diamond indenter, with a tip radius of 120 nm (which is calculated through calibration process [28]), was used. Indentation tests were performed at loads ranging between 25 and 6000 μN, at room temperature. Loading and unloading segments were kept constant at 10 s each for all tests and at the maximum load holding time was 10 s to minimize the time-dependent effect. Hardness (H), reduced modulus (E_r) and stiffness (S) are calculated from the slope of the unloading curve with the use of Oliver and Pharr method [29]. The presented H and E_r values are the mean values of 7 repeated tests at the longitude of the samples at each applied load.

3. Results and discussion

3.1. Morphological analysis

SEM and AFM analyses were employed aiming at evaluating the morphology and the topography as well as the quality of the film surfaces. The SEM analysis revealed that, in all cases, dense coatings, exhibiting a defect-free surface without any pores or microcracks, were developed. Representative SEM images of the coatings' surfaces

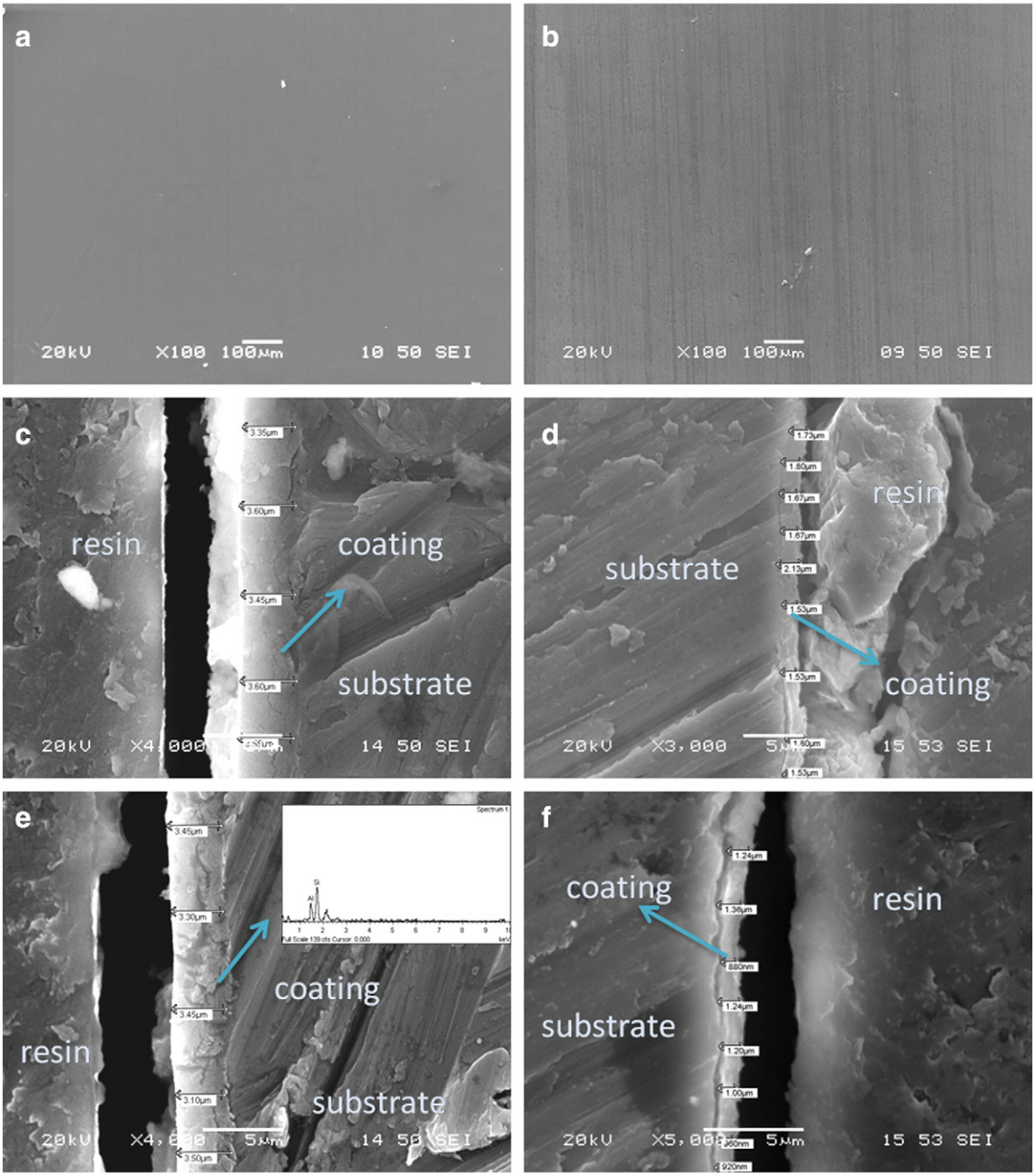

Fig. 1. Scanning secondary electron images of coating surface, coating–aluminum interface and energy dispersive spectroscopy (EDS) analysis for: a) PEI25000-300, b) PEI25000-100, c) PEI25000-300, d) PEI25000-100, e) PEI25000-MBI-300 and f) PEI25000-MBT-100 coated coupons.

are depicted in Fig. 1a and b. Films are dense and of high quality as a result of the presence of the organic component in sols, which render the gel network more flexible and less susceptible to cracking [30]. Similarly, the SEM images of the cross-sections of the coated coupons (Fig. 1c–f) demonstrated the high quality of the coating–aluminum interface, since irrespectively of the dipping time into the silane sol the as developed films appear homogeneous with good adhesion to the substrate.

The essential adhesion of the synthesized coatings can be attributed to the fact that the film is 'cross-linked' and stably attached on Al surface both through covalent and non-covalent, but rather strong, interactions of amino groups with silica and alumina active sites [5–31], providing thus an insoluble protective, adherent layer on the substrate. The character of bond interactions of the coating layer with the Si–OH groups and the Lewis acid sites of alumina of the metal substrate has been established by FTIR analysis in our previous work [18] and is also discussed in detail elsewhere [5–31]. Further, inhibitors that consist of functional groups (such as $-NH_2$, $-OH$, $-SH$, $-COOH$ and $-SO_3H$) [32], form stable five- or six membered chelate rings [33], enhancing and strengthening coating chemisorption. The availability of non-bonded (lone pair) and p-electrons in such inhibitor molecules facilitates the electron transfer from the inhibitor to the metal. A coordinate covalent bond involving transfer of electrons from inhibitor to the metal surface may be formed. The strength of the chemisorption bond depends on the electron density on the donor atom of the functional group and also on the polarizability of the group [34].

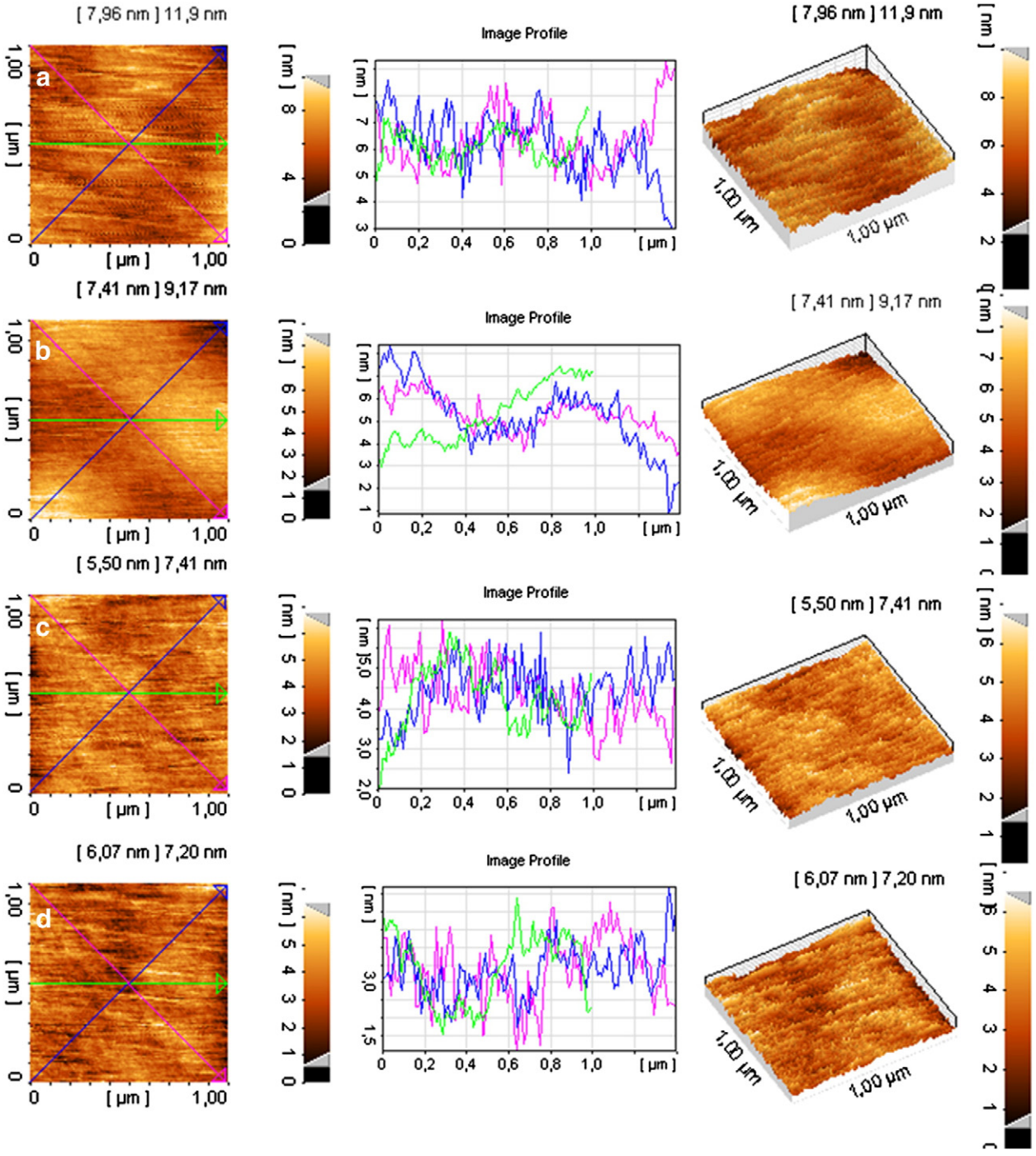

Fig. 2. AFM images showing height and phase (1 × 1 µm) of the surface morphology for: a) PEI25000-100, b) PEI25000-300, c) PEI25000-MBI-100 and d) PEI25000-MBI-300.

As can be seen in Fig. 1, the average thickness for the coatings of 100 s dipping period is about 1–1.5 μm whereas that of the coatings of 300 s is about 3–3.5 μm, respectively, suggesting a dependence of the coating thickness on the residence time in the cross-linked silane sol. This behavior can be attributed to the cross-linking process that is continued during the whole dipping period increasing by this way the thickness of the layers that is formed. This result is independent of the solution final formulation as the presence or absence of the corrosion inhibitor in the solution did not affect the coating's thickness.

Fig. 2 shows the AFM micrographs of the surface morphology for the PEI inhibitor-free coatings and PEI–MBI coatings prepared after dipping in the silane sol either for 100 s (leading to a coating thickness of 1–1.5 μm as discussed above) or 300 s (with a final coating thickness of 3–3.5 μm). The surface roughness in all cases is in the range of few nm; however, it seems that the coatings containing MBI are slightly smoother with an average roughness of 5.5–6 nm compared to an average roughness of 7.5–8 nm measured for the inhibitor free coatings. In contrast, the final thickness of the coatings does not seem to affect the roughness.

3.2. Anticorrosion protection evaluation

3.2.1. PDS results

Potentiostatic polarization curves of coated coupons in Harrison's solution, prepared for a dipping period of 100 s of the alloy samples in the silane sol, are presented in Fig. 3. In the same figure the polarization curve of bare aluminum alloy is also shown for comparison. Measurements for coated coupons were performed after 90 min immersion in the Harrison's solution, whereas the immersion period for bare aluminum alloy was 20 min.

As can be seen, the corrosion potential E_{corr} for all coated samples has become more positive in comparison to E_{corr} corresponding to bare aluminum alloy, indicating a reduced tendency to corrosion, as expected. Moreover, the current density of coated samples is considerably smaller than that of bare aluminum alloy within the whole potential range, demonstrating a reduced rate of redox reactions on the metal substrate. Additional information on the anticorrosion properties of the coating can be obtained by determining the corrosion current i_{corr} by Tafel extrapolation. Even though, determining i_{corr} from complex potentiodynamic curves, as those presented in Fig. 3, is rather implausible, a comparative evaluation is possible. Thus, by comparing the values tabulated in Table 2, it can be observed that samples containing organic inhibitors possess better anticorrosion properties

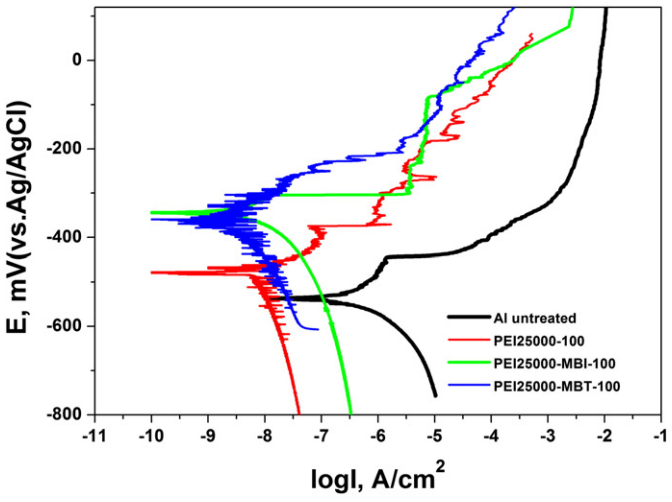

Fig. 3. Potentiodynamic scans for coated AA2024 alloy samples in Harrison's solution for untreated Al, PEI25000-100, PEI25000-MBI-100 and PEI25000-MBT-100.

Table 2
Potentiodynamic results of the synthesized coatings.

Coating code	E_{corr} (mV)	i_{corr} (nA/cm^2)
Al untreated	−537	486
PEI25000-100	−512	51
PEI25000-MBI-100	−344	16
PEI25000-MBT-100	−357	10
PEI25000-300 [18]	−380	6
PEI25000-MBI-300 [18]	−271	8
PEI25000-MBT-300 [18]	−297	1

since the corresponding i_{corr} values are smaller. This is in agreement with previous results showing that MBI and MBT present effective corrosion inhibition thus reducing localized corrosion currents [35]. The inhibitory action of these molecules can be attributed to the O, S and N atoms existing in the organic ring which can be attached to the aluminum substrate and block active corrosion sites [36]. O, N and S, due to their relatively high basicity and electron density, are the active centers for the process of adsorption of the inhibitor molecule on the metal surface. The use of organic compounds containing oxygen, sulfur and especially nitrogen as corrosion inhibitors to reduce corrosion attack has been studied in some detail on steel. The existing data show that most organic inhibitors are adsorbed on the metal surface by displacing water molecules, forming in this way a barrier that may involve transfer of electrons from the inhibitor to the metal surface due to the basicity of the functional groups of the inhibitor [34].

The above results are in full agreement with the results presented recently [18]; however, as in that work measurements concerned only coatings formed within a 300 s dipping period, the behavior is superior when compared to the results presented here. Thus, it can be concluded that the thickness of the coating is an important parameter since the data shown in the present work concern thinner coatings, exhibiting only the 1/3 of the thickness of the coatings presented in [18] (i.e. coatings obtained with the same procedure but with a dipping period of 300 s). The dependence of corrosion rate on the coating thickness can be assigned to the effective closure of any micropores as well as to the increase of the length of the diffusion path to the alloy surface. It should be also emphasized that for both thick and thin coatings containing an inhibitor, a very similar trend is observed, as always these coatings demonstrate the best behavior. Moreover, MBT exhibits relatively better anticorrosion inhibition performance compared to MBI.

The very good barrier properties of the coatings and the superior behavior of inhibitor containing ones were also confirmed in SEM studies of their surface after the PDS test (Fig. 4). In fact, the defects presented in the coating surfaces after the test are very limited with the lowest damage observed in the case of PEI-organic inhibitors coating systems which display very few and small microcracks.

3.2.2. EIS results

The Bode plots presented in Fig. 5 correspond to EIS measurements of organic inhibitor coated samples and inhibitor free coatings after immersion in Harrison's solution for 72 h. The impedance spectra depend at least on three factors: the conductivity of the electrolytic solution, the electrical properties of the sol–gel coating layer and the electrochemical properties of the metal/solution interface at the bottom of the coating. An additional factor may be the existence of a layer on the metal substrate due to the formation of aluminum oxide or hydroxide and its interaction with silicon groups existing in the silane sol [37]. The electrical properties of the electrolytic solution are irrelevant for the evaluation of the coating and are expected to be recorded at very high signal frequencies ($>10^4$ Hz). The electrical properties of the coating are revealed at intermediate frequencies. These are the coating resistance and capacitance. The former can be attributed to the resistance of the pores developed in the coating due to its porosity, whereas the latter to the water uptake of the

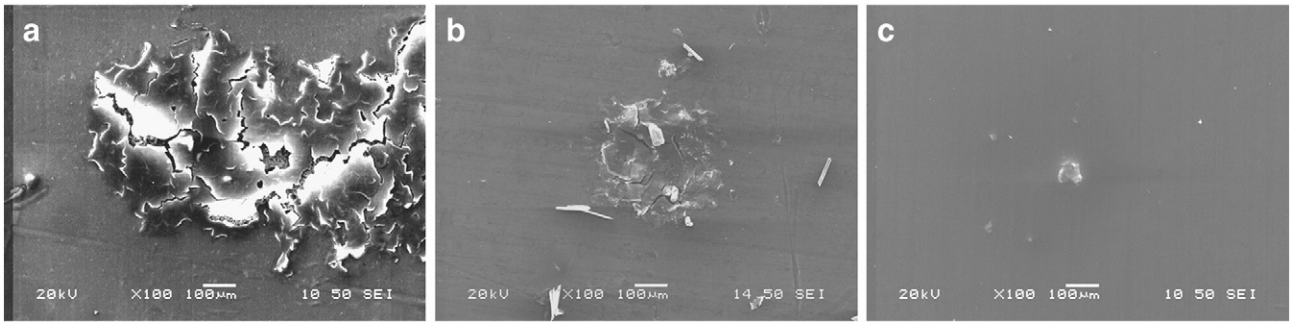

Fig. 4. Scanning secondary electron images of coatings after the PDS tests for: a) PEI25000-100, b) PEI25000-MBI-100 and c) PEI25000-MBT-100.

undamaged coating. Finally, at very low frequencies, the electrochemical properties of the metal/solution interface can be determined, concerning the corrosion resistance of the metal and the double layer capacitance.

As can be seen from the modulus plot Z_{mod} of Fig. 5 (red curve), the inhibitor-free coating exhibits a relatively higher coating resistance but the corrosion resistance at the metal/solution interface is lower when compared to the coatings containing MBI (green curve) or MBT (blue curve) (exhibiting the lowest pore resistance among all the films). In both cases of inhibitor-free and inhibitor-containing films the coating capacitance seems to be similar and thus the water absorption must be comparable. The initiation of the processes related to the metal/solution interface is evident also from the phase angle plot where two time constants are recorded. However, the separation of the time constants is not evident in the coating containing MBT (blue curve), so clear conclusions for the electrical properties of the coating cannot be drawn. Nevertheless, since the value of Z_{mod} at low frequencies is relatively high and very similar to the Z_{mod} of MBI-coating, it can be concluded that the corrosion rate for this sample is also reduced.

The coating containing MBT is further explored by measuring the impedance spectra as a function of time. In Fig. 6 the corresponding Bode plots are presented after 72 h, 1, 2, 3 and 4 weeks of immersion in Harrison's solution. As can be seen, after 72 h of immersion (black curve) a single time constant is observed. Thus, it can be assumed that either a separation of the time constants related to the coating and the double layer is not evident or that the impedance spectrum corresponds to a coating developing a resistance due to low porosity. In any case, the impedance value at small frequencies is high, a clear indication that the corrosion rate is low. After one and two weeks of immersion (red and green curves) the time constant recorded at intermediate frequencies (the slope of the Z_{mod} curve recorded between 10^2 and 1 Hz) remains the same, but the impedance at small frequencies is decreased. This fact together with the indication of an additional time scale at small frequencies in the phase angle plot demonstrates the initiation of corrosion on the metal substrate. The blue curve corresponds to the impedance measurement after three weeks of immersion. Even though the capacitance at intermediate frequencies remains the same, the value of Z_{mod} at low frequencies increases. This trend can be attributed to the release of the corrosion inhibitor from the sol–gel matrix to the substrate. As detailed in [18], during the contact between the corrosion medium and the intermetallic surface, hydrolysis of Al and Mg leads to the electrochemical evolution of H_2 together with O_2 reduction, which result to a local pH increase [15–25] and may provoke the inhibitor release around the formed defect [15]. Thus, a thin absorption layer which hinders the expansion of corrosion phenomena, is formed on the damaged metallic surface [15]. The effect is more evident after four weeks of immersion (cyan curve) where the impedance value corresponding to the corrosion process remains high even though the electrical characteristics of the coating are poorer (i.e. lower pore resistance and higher coating capacitance).

A similar behavior is observed also for the coating containing MBI (data not shown), in accordance with the results obtained previously [18] revealing self-healing behavior. However, the impedance values measured in the present work are in all cases lower compared to those observed in the aforementioned work [18]. This result is directly assigned to the smaller thickness of the coatings measured here in complete agreement with the PDS results described above which proved the effect of thickness on the corrosion protection provided.

3.3. Nanoindentation analysis results

Indentation tests were initially performed on the AA2024-T3 substrate and revealed H and E_r values of 3 GPa and 50 GPa, respectively

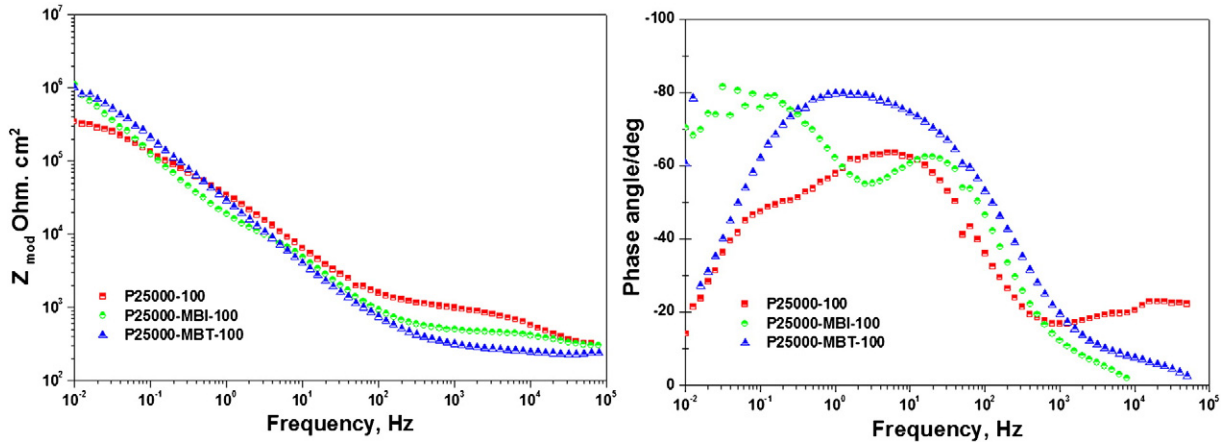

Fig. 5. Bode plots for coated AA2024-T3 alloy samples in Harrison's solution for immersion time 72 h for PEI25000-100, PEI25000-MBI-100 and PEI25000-MBT-100.

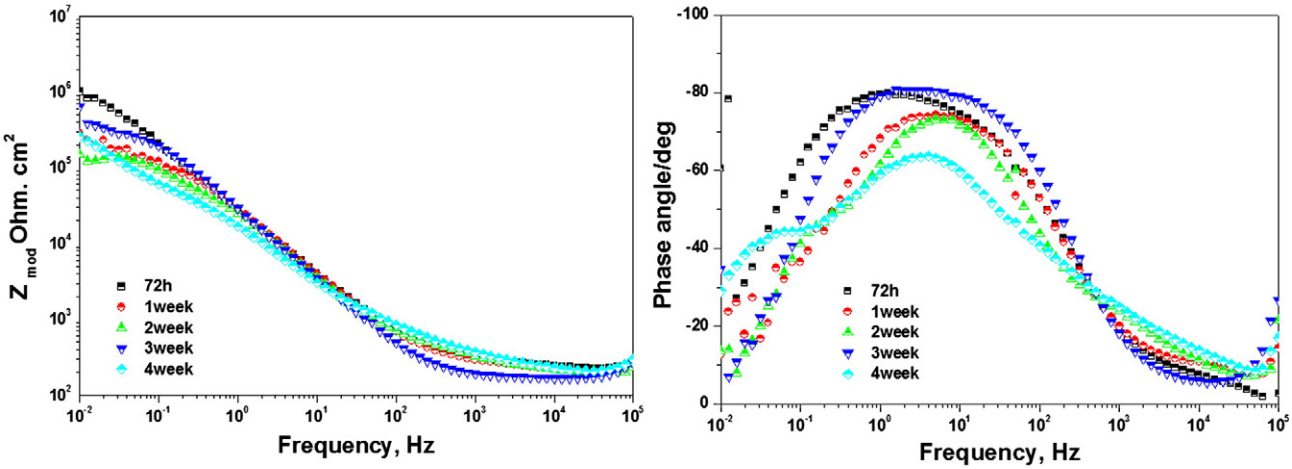

Fig. 6. Bode plots for AA2024-T3 aluminum alloy coated with PEI25000-MBT-100 immersed in Harrison's solution for different time periods.

[38]. All the as-developed coatings were then tested and the obtained load–unload curves were analyzed in order to evaluate the nanomechanical properties and explain coating plastic deformation. At low applied loads ($F = 25$ μN) it is observed that all coatings reveal elastoplastic behavior and the indenter reaches approximately the same indentation depths (inset graphs of Fig. 7). Additionally, it is noted that 100 s and 300 s dip coated samples exhibit the same behavior, because at shallow indentation depths (<10% of coating

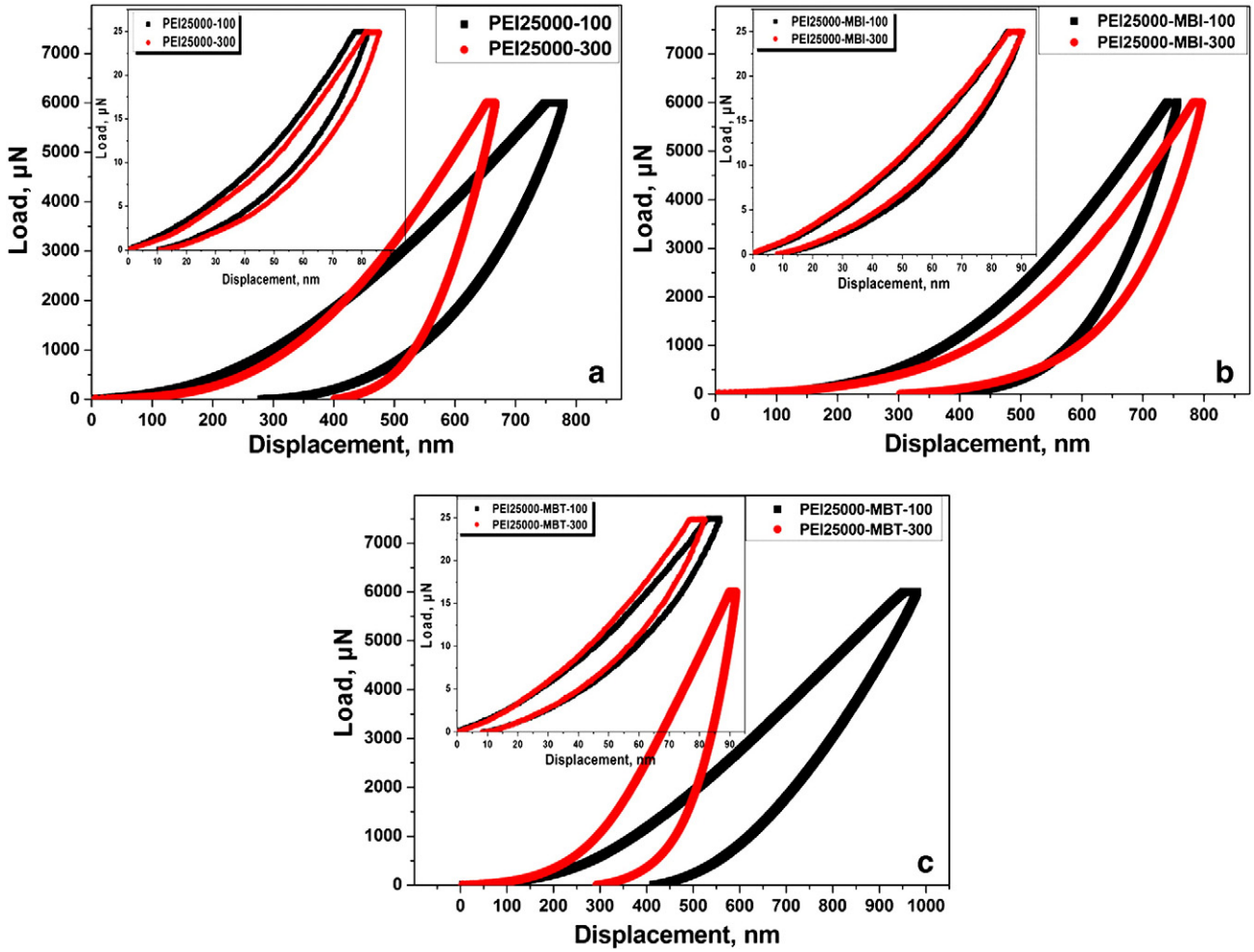

Fig. 7. Typical load–unload curves obtained for: (a) PEI25000-100 and PEI25000-300, (b) PEI25000-MBI-100 and PEI25000-MBI-300 and (c) PEI25000-MBT-100 and PEI25000-MBT-300 at applied load 6000 μN. Inset graphs represent the load–unload curves at applied load 25 μN of the respective samples.

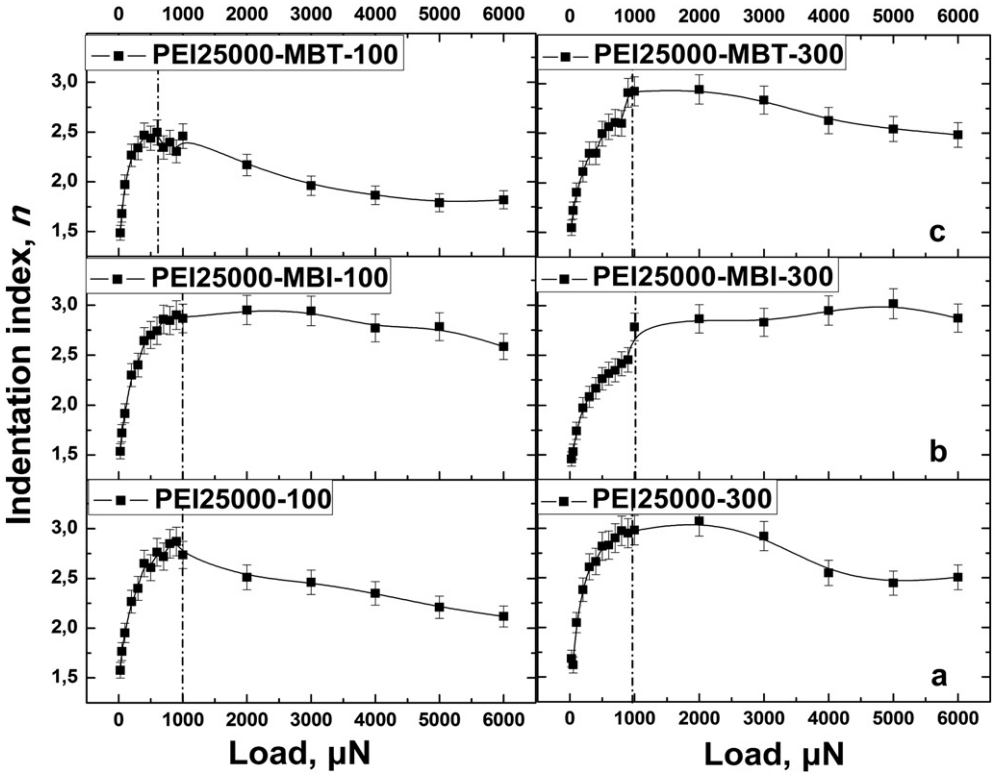

Fig. 8. Indentation index, *n*, values as a function of applied load for: (a) PEI25000-100 and PEI25000-300, (b) PEI25000-MBI-100 and PEI25000-MBI-300 and (c) PEI25000-MBT-100 and PEI25000-MBT-300.

thickness) substrate effects are negligible permitting the clear evaluation of coatings' nanomechanical properties [39]. At higher applied loads ($F = 6000$ μN) it is observed that 300 s dip coated samples present higher resistance to compressive forces, with the exception of PEI25000-MBI-300 which shows a quite similar behavior to the respective coating of 100 s.

Slope changes that are observed at loading curves are studied through a power law relation, by which loading data are fitted through

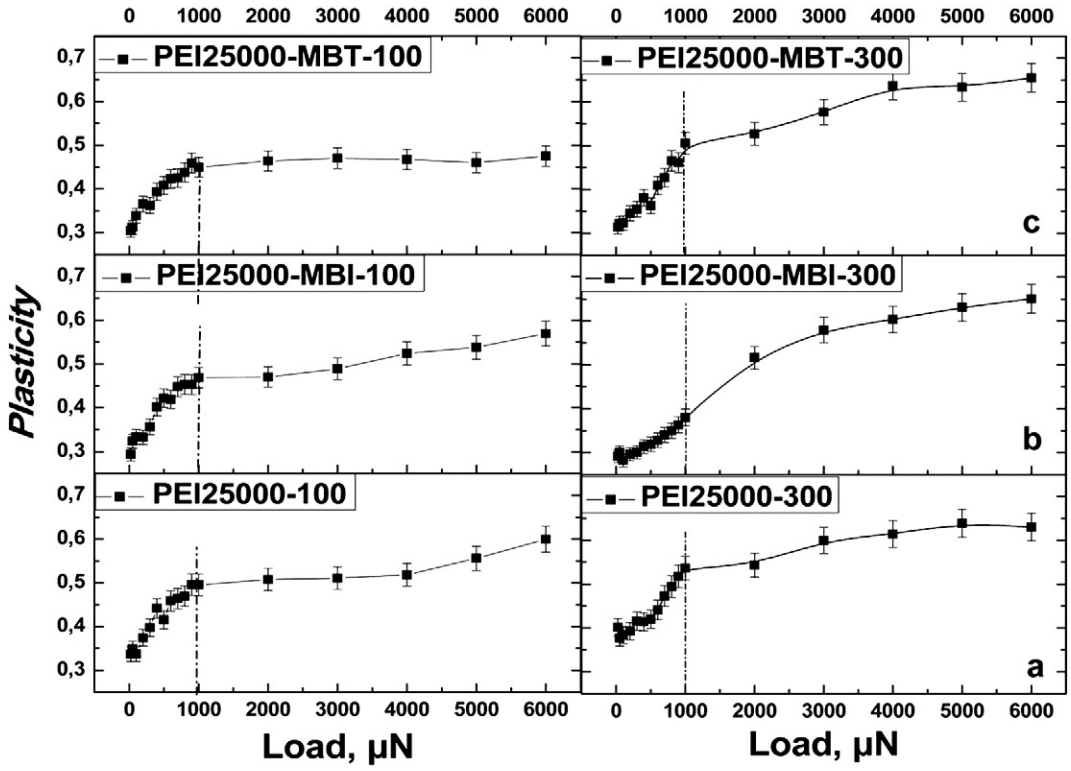

Fig. 9. Plasticity values as function of applied load for: (a) PEI25000-100 and PEI25000-300, (b) PEI25000-MBI-100 and PEI25000-MBI-300 and (c) PEI25000-MBT-100 and PEI25000-MBT-300.

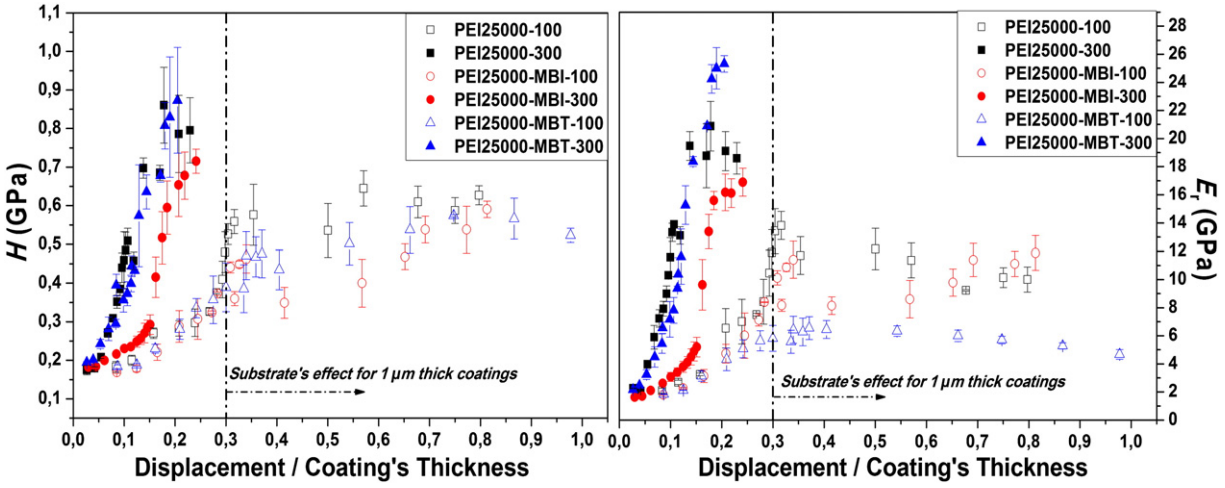

Fig. 10. Hardness (H) and reduced modulus (E_r) values as a function of displacement/coating's thickness, for all tested coatings.

the general relationship between the applied load (P) and the penetration depth (h) of an indenter (Eq. (1)) [40]:

$$P = ah^n \tag{1}$$

where the constants a and n are geometric and material parameters, respectively. Factor n is a measure of the material's resistance to deformation and it is called 'indentation index'. Fig. 8 depicts the calculated n values, obtained by the fitting of the loading curves at all applied loads, via the power law in Eq. (1). It is observed that n values are approximately equal for all tested samples and present the same trend. Indentation index values increase with increasing applied load, reaching a maximum value at applied load 1000 μN for all tested samples. The load of 1000 μN indicates a theoretical transition of the elastic to plastic

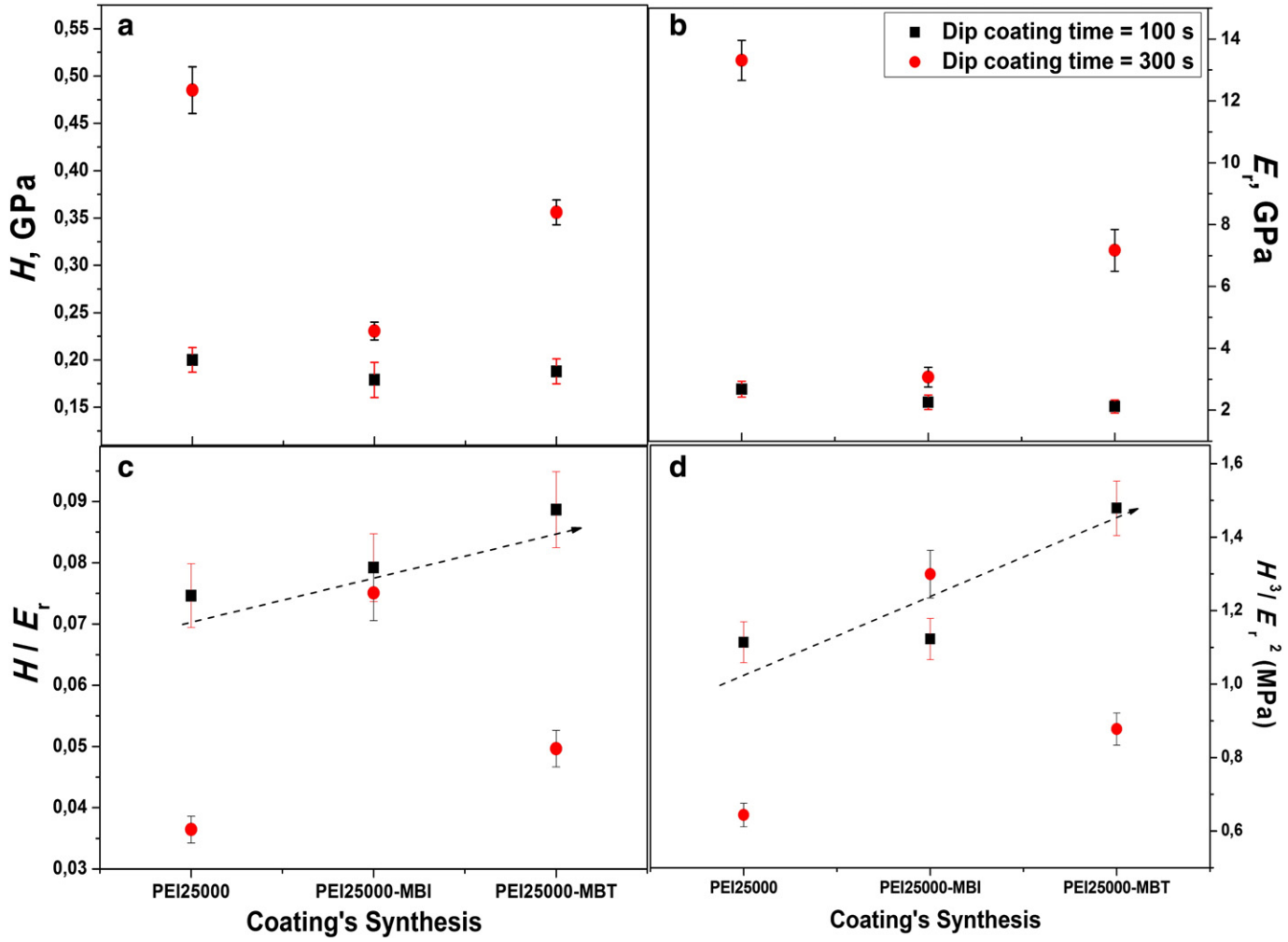

Fig. 11. (a) Hardness, (b) reduced modulus, (c) H/E_r and (d) H^3/E_r^2 values for the different synthesized coatings at 10% of coatings' thickness.

behavior of the tested samples. The maximum n values vary between 2.5 and 3 revealing the viscous behavior of the synthesized coatings. Further increase in applied load results in the decrease of the n values, which is more pronounced for the 100 s dip coated samples, due to the AA2024-T3 substrate effect. In general, 300 s dip coated samples present slightly higher n values, thus more viscous behavior, attributed to the more bulky structure of the hybrid organo-silicate coatings, compared to 100 s dip coated samples. Among them PEI25000-MBT-100 coating exhibits the lowest n values, probably attributed to higher effect of the aluminum substrate, possibly because of the better adherence of coating to the aluminum substrate [41].

Further analysis of the obtained load − unload curves indicate the theoretical shear strength of the synthesized samples. The theoretical shear strength indicates the limit of the restoring force (Plasticity), i.e. the boundary where no further increase is observed with increasing applied load (or displacement) [42]. The coatings' Plasticity at different applied loads was calculated by integrated areas under the loading (A_{total}) and the unloading curve ($A_{unloading}$) via (Eq. (2)):

$$\text{Plasticity} = \frac{A_{total} - A_{unloading}}{A_{total}}. \quad (2)$$

Fig. 9 presents the evolution of the calculated Plasticity values with applied load. Generally, small displacements are equivalent to a linear-elastic response and larger displacements elicit a non-linear response; consequently, it is depicted in Fig. 9, that the theoretical transition from elastic to plastic deformation is exhibited at 1000 μN for all samples, as it was previously presented for the indentation index values (Fig. 8). In Fig. 9, it is observed that at low applied loads, the coatings reveal elastoplastic behavior, while increasing applied load enhances Plasticity values. This increase is lower for the 100 s dip coated samples due to the AA2024-T3 substrate effect.

Fig. 10 depicts the hardness (H) and reduced modulus (E_r) values of all tested coatings as a function of the displacement/coating's thickness ratio. It is observed that thicker coatings present higher H and E_r values compared to 100 s dip coated samples. Additionally, 300 s dip coated samples exhibit a continuously increasing trend in H and E_r values, because substrate effect is negligible. On the contrary, 100 s dip coated samples present a plateau in the measured H and E_r values due to the aluminum substrate effect, since the performed indentation tests reached coating–substrate interface. Furthermore, it is observed that the addition of MBI and/or MBT inhibitors for both 100 s and 300 s dip coated coatings leads to a slight reduction of the measured H and E_r values, suggesting an improvement of the SiO_2 network flexibility.

Fig. 11 presents an overall graph of the mechanical properties of all samples at the 10% of coatings thickness, in order to eliminate substrate effect [39]. It is again evident in Fig. 11a and b that 300 s dip coated samples exhibit higher H and E_r values than the 100 s dip coated samples, however this difference is reduced with the addition of the organic inhibitors. Chen et al. claimed that organo-silicate coatings' H and E_r values are enhanced when the cross-linking degree of the polysiloxane oligomer is increased [43]. Possibly the addition of the organic inhibitors in the system could have affected the condensation rate and thus the cross-linking degree of the silica network resulting in a more flexible film. However, this assumption is out of the scope of this work and needs further investigation.

In Fig. 11c and d, the H/E_r and H^3/E_r^2 ratios at the 10% of coatings' thickness are presented. The H/E_r ratio has been previously used to rank materials in respect of their wear resistance [44–46], whereas H^3/E_r^2 ratio describes the amount of elasticity exhibited by a coating; i.e., high (low) H^3/E_r^2 values indicate an elastic (plastic) behavior of the coating [28–50]. In Fig. 11c showing the H/E_r ratio it is observed that 100 s dip coated samples present better wear resistance, compared to 300 s dip coated samples and that in both cases the addition of the corrosion inhibitors improves this property. Furthermore, the H^3/E_r^2 ratio (Fig. 11d) revealed a similar trend: the thinner coatings present in general a more elastic behavior compared to thicker coatings and the addition of MBI and MBT inhibitors improves this property as well.

4. Conclusions

Hybrid organo-silicate anticorrosive coatings were deposited onto aluminum alloy substrates through an aqueous sol–gel method that employs hyperbranched poly(ethylene imine) to cross-link the silica network onto the metal surface as well as to solubilize corrosion inhibitors to get integrated into the deposited film. Coatings of two different thicknesses (1–1.5 and 3–3.5 μm, respectively) were produced by varying the dipping time into the silanes' sol.

In all cases, smooth coatings of high quality with good corrosion barrier properties were obtained, whereas the integration of an organic inhibitor into the film induces self-healing behavior. The coating thickness is a parameter that affects anticorrosion performance, since the thinner coatings of 1–1.5 μm demonstrate slightly inferior behavior. It should be emphasized, however, that even these coatings present satisfactory self-healing ability when a corrosion inhibitor is included.

The analysis of the nanomechanical properties revealed that the coatings are quite flexible with a viscous behavior attributed to their organic content. In fact, the measurements showed that the indentation index increases with the applied load, reaching, in all cases, its maximum value at 1000 μN. The maximum value was evaluated varying between 2.5 and 3 for the different coatings suggesting their viscous behavior, whereas the load of 1000 μN can be considered as the coating's theoretical transition point of the elastic to plastic behavior. Further, the analysis of the hardness and reduced modules of coatings showed slightly superior behavior of the thinner coatings compared to the thicker ones, since in general they present a more elastic behavior. More interestingly, however, the nanoindentation analysis demonstrated that the integration of either the MBI or the MBT inhibitor into the network, leads to coatings with at least similar or even improved overall nanomechanical performance.

References

[1] E.P. Plueddemann, Silane Coupling Agents, Plenum Press, New York, 1982.
[2] C.J. Brinker, G.W. Scherer, Sol–Gel Science: The Physics and Chemistry of Sol–Gel Processing, Academic Press, San Diego, CA, 1990.
[3] Y. Liu, D. Sun, H. You, J.S. Chung, Appl. Surf. Sci. 246 (2005) 82.
[4] A. Atkinson, D.L. Segal, J. Sol–Gel. Sci. Technol. 13 (1998) 133.
[5] V. Palanivel, Y. Huangb, W.J. van Ooij, Prog. Org. Coat. 53 (2005) 153.
[6] M.L. Zheludkevich, I.M. Salvado, M.G.S. Ferreira, J. Mater. Chem. 15 (2005) 5099.
[7] M.S. Donley, R.A. Mantz, A.N. Khramov, V.N. Balbyshev, L.S. Kasten, D.J. Gaspar, Prog. Org. Coat. 47 (2003) 401.
[8] S.K. Poznyak, L.M. Tedim, A.N. Rodrigues, M.L. Salak, L.F.P. Zheludkevich, M.G.S. Dick, Ferreira ACS Appl. Mater. Interfaces 1 (2009) 2353.
[9] A. Wittmar, M. Wittmar, A. Ulrich, H. Caparrotti, M. Veith, J. Sol–Gel Sci. Technol. 61 (2012) 600.
[10] M. Kendig, M. Hon, Electrochem. Solid-State Lett. 8 (2005) B10.
[11] A. Yabuki, H. Yamagami, K. Noishiki, Mater. Corros. 58 (2007) 497.
[12] N.N. Voevodin, N.T. Grebasch, W.S. Soto, F.E. Arnold, M.S. Donley, Surf. Coat. Technol. 140 (2001) 24.
[13] S.V. Lamaka, M.L. Zheludkevich, K.A. Yasakau, M.F. Montemor, P. Cecílio, M.G.S. Ferreira, Electrochem. Commun. 8 (2006) 421.
[14] E.V. Skorb, D. Fix, D.V. Andreeva, H. Möhwald, D.G. Shchukin, Adv. Funct. Mater. 19 (2009) 2373.
[15] D.G. Shchukin, M. Zheludkevich, K. Yasakau, S. Lamaka, M.G.S. Ferreira, H. Möhwald, Adv. Mater. 18 (2006) 1672.
[16] A.N. Khramov, N.N. Voevodin, V.N. Balbyshev, R.A. Mantz, Thin Solid Films 483 (2005) 191.
[17] A.N. Khramov, N.N. Voevodin, V.N. Balbyshev, M.S. Donley, Thin Solid Films 447 (448) (2004) 549.
[18] E. Roussi, A. Tsetsekou, D. Tsiourvas, A. Karantonis, Surf. Coat. Technol. 205 (2011) 3235.
[19] B.E. Rivas, K.E. Geckeler, Adv. Polym. Sci. 102 (1992) 171.
[20] M. Finsgar, S. Fassbender, Nicolini, I. Milosev, Corros. Sci. 51 (2009) 525.
[21] M. Arkas, L. Eleades, C.M. Paleos, D. Tsiourvas, J. Appl. Polym. Sci. 97 (2005) 2299.
[22] M. Arkas, D. Tsiourvas, J. Hazard. Mater. 170 (2009) 35.

[23] T.L. Metroke, E.T. Knobbe, Materials Research Society Symposium—Proceedings, Organic/Inorganic Hybrid Materials, San Francisco, 628, 2000, p. CC11.4.1.
[24] T.L. Metroke, R.L. Parkhill, E.T. Knobbe, Prog. Org. Coat. 41 (2001) 233.
[25] M.L. Zheludkevich, R. Serra, M.F. Montemor, I.M. Salvado, M.G.S. Ferreira, Surf. Coat. Technol. 200 (2006) 3084.
[26] R. Twite, S. Balbyshev, G. Bierwagen, Proc. Symp. Environ. Accept. Inh. Coat, Special Publication of the Electrochemical Society, 1997. 202.
[27] A.N. Chamos, C.A. Charitidis, A. Skarmoutsou, Sp.G. Pantelakis, Fatigue Fract. Engn. Mater. Struct. 33 (2010) 252.
[28] C.A. Charitidis, Int. J. Refract. Met. Hard Mater. 28 (2010) 51.
[29] W.C. Oliver, G.M. Pharr, J. Mater. Res. 7 (1992) 1564.
[30] J.S. Park, J.D. Mackenzie, J. Am. Ceram. Soc. 78 (1995) 2669.
[31] C.K. Nmai, Cem. Concr. Compos. 26 (2004) 199.
[32] A. Luttringaus, Angew. Chem. 64 (1952) 661.
[33] D.C. Zecher, Mater. Perform. 15 (1976) 33.
[34] B.E. Amitha Rani, Bharathi Bai J. Basu, Intl. J. Corros. 10 (1155) (2012) 380217.
[35] S.X. Zhneg, J.H. Li, J. Sol–Gel Sci. Technol. 54 (2010) 174.
[36] B. Sanyal, Prog. Org. Coat. 9 (1981) 165.
[37] M.L. Zheludkevich, R. Serra, M.F. Montemor, K.A. Yasakau, I.M. Miranda Salvado, M.G.S. Ferreira, Electrochim. Acta 51 (2005) 208.
[38] E.P. Koumoulos, D.A. Dragatogiannis, C.A. Charitidis, Nanomechanical Analysis of High Performance MaterialsDr. Atul Tiwari, Springer, 2012.
[39] R. Saha, W.D. Nix, Acta Mater. 50 (2002) 23.
[40] Q. Ma, D.R. Clarke, J. Mater. Res. 104 (1995) 853.
[41] B. Sanyal, Prog. Org. Coat. 9 (1981) 165.
[42] U.F. Kocks, C.N. Tome, H.R. Weng, Texture and Anisotropy, Cambridge University Press, 1998.
[43] X. Chen, S. Zhou, B. You, L. Wu, J. Sol–Gel Sci. Technol. 58 (2011) 490.
[44] L. Oberle, J. Met. 3 (1951) 438.
[45] J. Halling, Tribol. 1 (1982) 15.
[46] A. Leyland, A. Matthews, Wear 246 (2000) 1.
[47] C. Rebholz, A. Leyland, J.M. Schneider, A.A. Voevodin, A. Matthews, Surf. Coat. Technol. 120–121 (1999) 412.
[48] P. Favia, G. Cicala, A. Milella, F. Palumbo, P. Rossini, R. d'Agostino, Surf. Coat. Technol. 169–170 (2003) 609.
[49] C. Charitidis, S. Logothetidis, P. Douka, Diamond Relat. Mater. 8 (1999) 558.
[50] E. Le.Bourhis, Vacuum 82 (2008) 1353.